CHEMISTRY OF MATERIALS

Article

pubs.acs.org/cm

Self-Assembly of Pluronic F127—Silica Spherical Core–Shell Nanoparticles in Cubic Close-Packed Structures

Stef Kerkhofs,[†] Tom Willhammar,[‡] Heleen Van Den Noortgate,[†] Christine E. A. Kirschhock,[†] Eric Breynaert,[†] Gustaaf Van Tendeloo,[‡] Sara Bals,[‡] and Johan A. Martens*[,†]

[†]Centre for Surface Chemistry and Catalysis, KU Leuven, Kasteelpark Arenberg 23, 3001 Leuven, Belgium

[‡]Electron Microscopy for Materials Science (EMAT), University of Antwerp, Groenenborgerlaan 171, 2020 Antwerpen, Belgium

Supporting Information

ABSTRACT: A new ordered mesoporous silica material (COK-19) with cubic symmetry is synthesized by silicate polycondensation in a citric acid/citrate buffered micellar solution of Pluronic F127 triblock copolymer near neutral pH. SAXS, nitrogen adsorption, TEM, and electron tomography reveal the final material has a cubic close packed symmetry ($Fm\bar{3}m$) with isolated spherical mesopores interconnected through micropores. Heating of the synthesis medium from room temperature to 70 °C results in a mesopore size increase from 7.0 to 11.2 nm. Stepwise addition of the silicate source allows isolation of a sequence of intermediates that upon characterization with small-angle X-ray scattering uncovers the formation process via formation and aggregation of individual silica-covered Pluronic micelles.

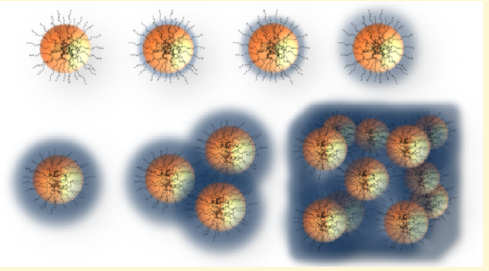

INTRODUCTION

Ordered mesoporous silica (OMS) materials have arrays of identical mesopores separated by amorphous silica walls. The uniformity of the mesopores and the walls is particularly attractive for a variety of applications including catalysis, pharmaceutical formulation, and microelectronics.[1−9] OMS materials are created by a supramolecular assembly process of silicate molecules and surfactant. The cooperative self-assembly of individual surfactant and silicate molecules is one of the proposed formation mechanisms.[10−13] Silica precipitation on prearranged surfactant micelles, fulfilling a role of liquid crystal templates, is an alternative model.[13−16] After evacuation of the surfactant molecules from the assembled material, mesopores separated by silica walls remain. Initially, OMS materials were synthesized from strongly alkaline or strongly acidic synthesis mixtures. Later, synthesis protocols were developed enabling synthesis at less extreme pH levels.[17−21] Particularly, pH-buffered solutions provide attractive options for mastering the formation process.

COK-12 is an example of an ordered mesoporous silica material prepared under slightly acidic, buffered conditions.[19,20] The synthesis of COK-12 starts from a citric acid/citrate buffered solution of amphiphilic triblock copolymer P123 ($EO_{20}PO_{70}EO_{20}$) which self-assembles into spherical micelles. Hydrophobic poly(propylene oxide) (PPO) chains form the hydrophobic core of the micelles, surrounded by a more hydrophilic layer of poly(ethylene oxide) (PEO) chains.[22−24] Silica preferentially infiltrates the outer PEO zone of the micelles, diminishing the mobility of the PEO chains and the sterical stabilization of the micelle dispersion. The infiltration of silica in the PEO layers triggers coalescence of the original micelles to form cylinders, which subsequently are arranged in a hexagonal packing. In this way, Pluronic P123 favors formation of hexagonally ordered platelet shaped OMS materials.[19] Its hexagonal mesostructure assembles spontaneously upon adding basic sodium silicate solution to a citric acid/citrate buffered Pluronic P123 triblock copolymer solution.[20] This formation mechanism was investigated by identifying the intermediate structures, which were prepared by limiting sodium silicate addition to the buffered P123 micelle suspension (Figure 1).[20]

F127 ($EO_{102}PO_{70}EO_{102}$) is a related triblock copolymer with substantially longer PEO blocks compared to P123

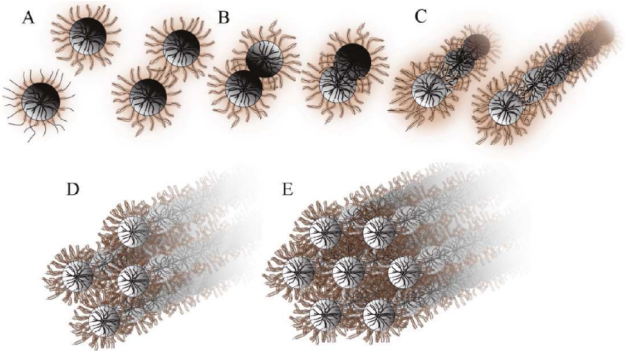

Figure 1. Schematic representation of the different stages in the formation of COK-12, a hexagonally ordered mesoporous silica. Reprinted with permission from ref 20. Copyright 2011 American Chemical Society.

Received: February 3, 2015
Revised: July 24, 2015
Published: July 24, 2015

DOI: 10.1021/acs.chemmater.5b01772
Chem. Mater. 2015, 27, 5161−5169

($EP_{20}PO_{70}EO_{20}$). Under dilute aqueous conditions, F127 polymer molecules self-assemble to spherical micelles with a hydrophobic core similar in size to that of spherical P123 micelles but with a thicker hydrophilic palisade layer due to the substantially longer PEO blocks.[12] F127 self-assembles into micelles with a hydrodynamic radius of approximately 8.0 to 12 nm and a core radius of 5.9 nm.[12,22,24] Previously, F127 was used for the synthesis of ordered mesoporous silica materials adopting body centered $Im3m$ symmetry, such as SBA-16[17,25] and face centered $Fm\bar{3}m$ symmetry in the instance of FDU-12[13,26−28] and KIT-5.[18,29] KIT-5 and FDU-12 are both synthesized using F127 as a template under different synthesis conditions and the use of different additives.[18,28,30] However, the SAXS diffraction patterns for both $Fm\bar{3}m$ materials differ substantially due to differences in pore configuration.[30]

Intrigued by the documented influence of the length of the PEO chains in the Pluronic template on the symmetry of the final silica material (cubic with F127, versus hexagonal with P123), we performed synthesis experiments with F127 in citric acid/citrate buffer and staged silicate addition to investigate the intermediates of this OMS formation process. Synthesis conditions leading to formation of a highly ordered new cubic phase designated as COK-19 were identified.

EXPERIMENTAL SECTION

Synthesis. A typical buffered F127 solution was prepared by dissolving 2.6 g of Pluronic F127 (BASF) in 107.5 g of deionized water. To this solution, 3.684 g of citric acid monohydrate (Sigma-Aldrich) and 2.540 g of trisodium citrate dihydrate (Sigma-Aldrich) were added. This buffered surfactant solution was stirred overnight to dissolve all components.

For the OMS material synthesis, 10.4 g of sodium silicate solution (27 wt % SiO_2, extra pure, Merck) diluted in 30 g of water was added to the buffered F127 solution at room temperature, while stirring vigorously. Precipitation of a white solid occurred instantaneously, and after 5 min of stirring, the suspension was kept under quiescent conditions to age for 24 h. Aging was done either at room temperature, 50 °C, or 70 °C. As-synthesized materials were filtered, washed, and dried at 50 °C. Finally, the powders were calcined in air at 350 °C for 24 h using a heating rate of 0.5 °C min^{-1}.

For the investigation of the assembly process with SAXS, flasks were filled with 3 g aliquots of buffered F127 solution. To these solutions, 0.15, 0.30, 0.40, 0.50, 0.60, 0.65, 0.7, 0.8, 0.90, and 1.00 mL of the diluted sodium silicate solution were added while stirring vigorously. These quantities correspond to 15, 30, 40, 50, 60, 65, 70, 80, 90, and 100% of the total sodium silicate amount of the typical COK-19 synthesis. SAXS patterns were recorded 5 min after mixing. pH increased from 3.6 in the buffered Pluronic solution to 3.8, 4.0, 4.1, 4.3, 4.4, 4.5, 4.5, 4.7, 4.8, and 5.0, respectively.

Characterization. Dynamic Light Scattering (DLS) analyses of suspensions were conducted in polystyrene cuvettes at 25 °C on a 90Plus instrument (Brookhaven Instruments Corporation), at a scattering angle of 90° using a 659 nm laser. The fluctuations in the scattered laser light intensity were correlated between 5 μs and 1 s. Correlation functions were analyzed with Igor Pro 6.2, using the Clementine package for modeling decay kinetics based on the Maximum Entropy method. The decay times were converted to hydrodynamic radii with the Stokes−Einstein relation, yielding intensity weighted size distributions. Viscosity values used in the Stokes−Einstein relation were adjusted by measuring viscosities using a rolling ball viscometer (Anton Paar).

Small-Angle X-ray Scattering (SAXS) of powder samples was recorded at room temperature using a SAXSess mc^2 instrument (Anton Paar) with line-collimated $Cu_{K\alpha}$ radiation and a 2D imaging plate detector in combination with a temperature controlled RotorCell sample stage. SAXS patterns were normalized to scattering intensity at higher angles. Background subtraction and desmearing were performed with the SAXSquant software.

To investigate the formation mechanism, the scattering profiles for synthesis mixtures with varying silicate concentrations were recorded using a 1 mm quartz capillary flow cell sample stage mounted in the SAXSess mc^2 instrument. The temperature was kept at 20 °C using a Peltier device (Anton Paar, TCS 120). SAXS patterns for the different mixtures were recorded over a time frame of 1 h. Ultrapure mQ water was used as a background. Modeling of the desmeared scattering curves was performed using Igor Pro 6.2 in combination with the NCNR SANS & USANS Data Reduction and Analysis package (v7.20).[31] The recorded SAXS patterns were fitted with a combined model, based on spherical core−shell particles and small dense particles with a Gaussian size distribution.[32] Synthesis mixtures containing larger amounts of sodium silicate were fitted with the same model, with pseudo-Voigt peaks superimposed. The pseudo-Voigt functions were introduced to best describe the peak shapes and are a combination of Lorentzian and Gaussian peak shapes.[33]

Nitrogen sorption isotherms were recorded on an Autosorb-1 apparatus (Quantachrome) at −196.8 °C. Prior to measurement, calcined samples were degassed at 150 °C for 13 h under reduced pressure. BET surface area was estimated in the P/P_0 region 0.05−0.3. Micropore volumes were estimated using the t-plot method. The pore size distribution was determined using NLDFT analysis. NLDFT models pore sizes are based on the nitrogen adsorption on a silica material with cylindrical pores smaller than 5 nm and spherical pores larger than 5 nm.

Scanning Electron Microscopy (SEM) and Scanning Transmission Electron Microscopy (STEM) images were recorded on a Nova NanoSEM450 (FEI). For SEM, samples were dispersed on carbon tape and measured without coating, using low voltages (0.5−1 kV) to reduce sample charging. In STEM mode, the device operated at 30 kV. STEM samples were prepared on 50 nm 300-mech carbon-coated copper grids.

High-Resolution Scanning Transmission Electron Microscopy (HRSTEM) images of the COK-19 crystals were acquired using an FEI Tecnai G2 operated at an accelerating voltage of 200 kV. The images were collected using a high angle annular dark field (HAADF) detector. The samples were crushed and dispersed in ethanol before a droplet of the dispersion was added to a carbon coated copper grid. For electron tomography, bright field TEM images was collected on an FEI Tecnai G2, operated at 200 kV. The tilt series of the sample aged at 70 °C covered angles between −72° and 76° and the series from the sample aged at room temperatures −76° to 76°. Both series were collected with a tilt increment of 2°. The tomographic reconstructions were performed using a SIRT algorithm, and the visualization was done with AMIRA.

^{29}Si magic angle spinning (MAS) NMR spectra were recorded using an AMX300 spectrometer (Bruker) operating at 100 MHz. 944 scans were accumulated with a recycle delay of 120s. Samples were packed in 4 mm zirconia rotors. Tetramethylsiliane was used as a chemical shift reference.

RESULTS AND DISCUSSION

Characterization of OMS Material. The addition of sodium silicate to the buffered Pluronic F127 solution led to the instantaneous formation of a white suspension. SAXS patterns of as-made materials indicated highly ordered materials (see Supporting Information, Figure S1). Drying and subsequent removal of the organic template by calcination resulted in porous material, coined COK-19. The calcined sample, prepared and aged at room temperature, shows well resolved diffraction lines indexed in an $Fm\bar{3}m$ symmetry as (111), (200), (220), and (311) with a unit cell parameter a = 21.9 nm (Figure 2). However, SAXS data alone are insufficient to determine meso-ordering in the structure.

Pore structure and long-range ordering were further investigated using transmission electron microscopy. High

DOI: 10.1021/acs.chemmater.5b01772
Chem. Mater. 2015, 27, 5161−5169

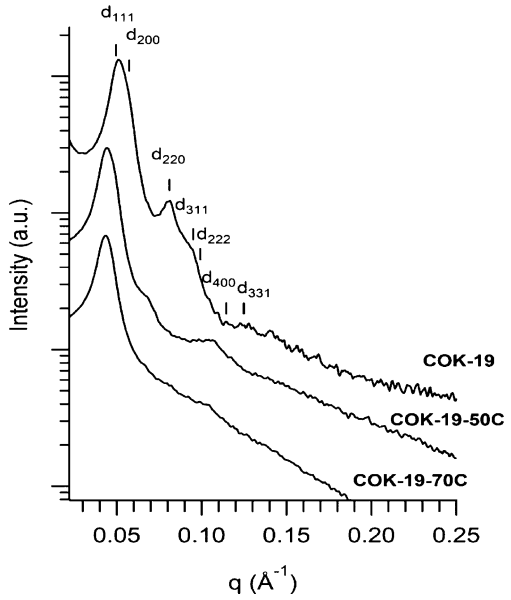

Figure 2. Small angle X-ray scattering patterns of COK-19 aged at room temperature, 50 or 70 °C and calcined at 350 °C. Diffraction peak positions are indicated by | .

angle annular dark field (HAADF) STEM images reveal the structure of an ordered mesoporous material consistent with the $Fm\bar{3}m$ structure (Figure 3). The images further show the presence of some stacking faults in COK-19 samples. As layers of close packed spheres are forming a three-dimensional

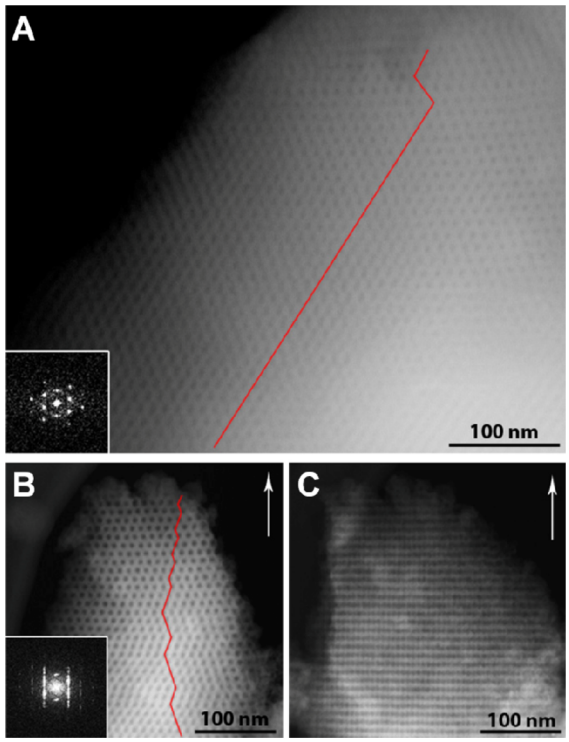

Figure 3. HAADF-STEM images of COK-19 (a) and COK-19-70C crystal (b, c). The COK-19-70C particle is rotated around the $[111]_c$ axis (marked by a white arrow). The particle is viewed along $[-110]_c$ (b) and $[-211]_c$ (c). The red line indicates the stacking (dis)order. Fourier transforms are shown as insets in a and b where streaks are characteristic for materials with stacking disorder.

structure, the layers can combine along the $[111]_c$ direction with two different sequences.[34,35] ABCA... stacking leads to cubic close packing (ccp), and ABA... stacking leads to hexagonal close packing (hcp).[36] A HAADF STEM image of a COK-19 particle aged at room temperature shows a large domain of cubic ordering, with some stacking faults near the rim of the particle (Figure 3A). An image from another particle exhibited a larger amount of stacking faults, suggesting some nonuniformity throughout the sample (see Supporting Information, Figure S2).

Scanning electron microscopy revealed the morphology of the calcined COK-19 as aggregates of truncated octahedrons with a mean diameter of approximately 500 nm to 3 μm (Figure 4). ^{29}Si MAS NMR analysis of the as-synthesized COK-

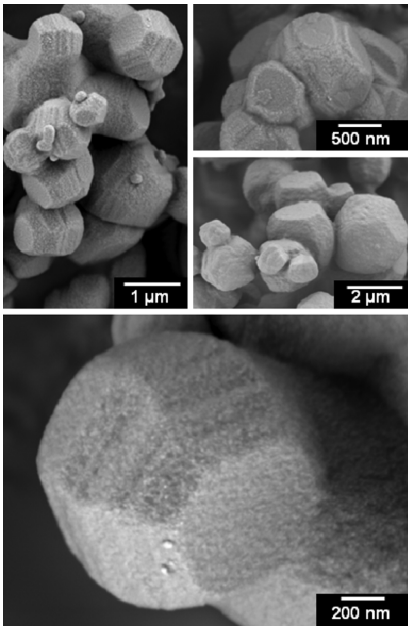

Figure 4. SEM micrographs of calcined COK-19.

19 material was performed to analyze the degree of condensation (see Supporting Information, Figure S8). The NMR spectra show the chemical environment around the silicon atom as $Si(OSi)_n(OH)_{4-n}$. Q^n represents Q^2, Q^3, and Q^4 signals at −92, −101, and −110 ppm respectively, with an intensity distribution of 9%, 42%, and 48%, indicating a condensed silicate network even at room temperature.

Freshly synthesized COK-19 suspensions were aged at 50 and 70 °C instead of room temperature for 24 h. Low angle diffractograms of calcined COK-19 materials aged at 50 and 70 °C resulted in less ordered material and caused the unit cell to increase to 25.9 and 27.2 nm, respectively (Figure 2). The structure loss was also apparent from HAADF images for COK-19-70C, aged postsynthesis at 70 °C (Figure 3B). This material has more stacking faults, which gives rise to streaks in the Fourier transform of the image. TEM is a method to study the local structure of selected particles. By combining the information from TEM with the results from SAXS, which provide averaged information from the entire sample, it can be confirmed that the sample aged at room temperature possesses a higher quality cubic ordering, with stacking faults increasing with temperature.

Heating causes considerable swelling of Pluronic micelles.[3,22,37] Aging above room temperature of the COK-19

DOI: 10.1021/acs.chemmater.5b01772
Chem. Mater. 2015, 27, 5161−5169

aggregates formed at room temperature introduced stacking faults in the material. The introduction of stacking disorders upon heating suggests that, in the initial colloids, the interaction between Pluronic core−silica shell particles is still largely physical, enabling alteration of stacking.

Besides line broadening through general lattice disorder, stacking faults in the $[111]_c$ direction also affect the SAXS pattern. Hcp intergrowths in a ccp structure influence line width and positions of certain reflections.[34,36] These stacking disorders, also known as intergrowths, occur more frequently for COK-19-70C as was seen with HAADF-STEM. COK-19-70C was aged at higher temperatures, where energetic differences between hcp and ccp packings become less deterministic. The increasing fraction of stacking disorder with temperature also explains the decreasing resolution of the low angle reflections in the SAXS curve with increasing aging temperature (Figure 2).[34]

COK-19 displayed a nitrogen physisorption isotherm with characteristics of both micro- and mesopores (Figure 5A, Table 1). The isotherm exhibits a hysteresis loop, characteristic for cage-type mesopores. The cage diameter is 7.0 nm, and the mesopore volume is 0.09 $cm^3\ g^{-1}$. The total pore volume of 0.29 $cm^3\ g^{-1}$ is mostly microporous (0.2 $cm^3\ g^{-1}$).

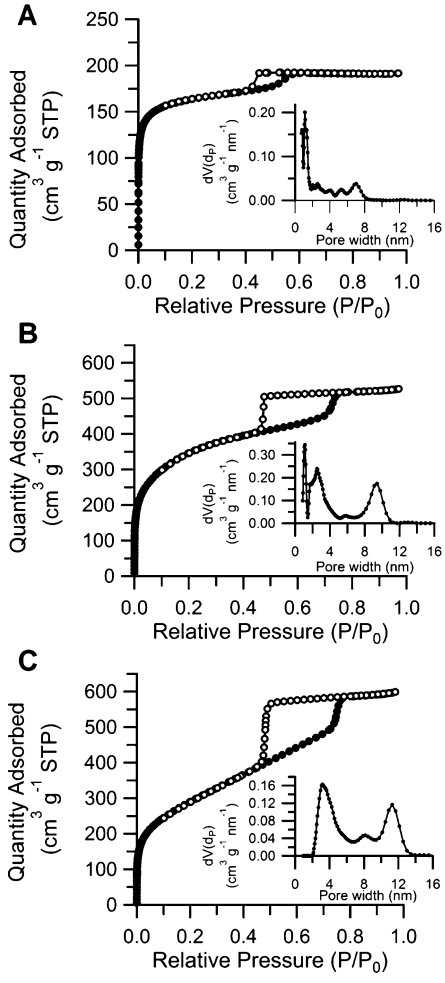

Figure 5. Adsorption (●) and desorption (○) branches of nitrogen physisorption isotherms of calcined (A) COK-19, (B) COK-19-50C, and (C) COK-19-70C. The insets show the pore size distribution based on NLDFT calculations.

Table 1. Synthesis, Structural, and Porous Properties of COK-19 Material Formed at Room Temperature, Aged at Different Temperatures, and Other $Fm\bar{3}m$ Structured Mesoporous Materials

	molar composition and synthesis condition								structural and porous properties						
samples	Si	template	swelling agent	KCl	citrate	HCl	H_2O	T^a (°C)	a^b (nm)	$d_{pore}{}^c$ (nm)	$W_t{}^d$ (nm)	BET (m^2g^{-1})	$V_t{}^e$ (cm^3g^{-1})	$V_{mi}{}^f$ (cm^3g^{-1})	
materials prepared with F127 as a template, without swelling agents															
COK-19	1	0.0044	0	0	0.56	0	163	18/18	22	7	8.5	514	0.29	0.2	[i]
COK-19−50C	1	0.0044	0	0	0.56	0	163	18/50	25.9	9.4	8.9	1187	0.78	0.46	[j]
COK-19−70C	1	0.0044	0	0	0.56	0	163	18/70	27.2	11.2	8	1035	0.88	0.25	[j]
KIT-5[18]	1	0.0035	0	0	0	0.88	119	45/45	17	6.8	5.2	390	0.21		
KIT-5[18,29]	1	0.0035	0	0	0	0.88	119	45/100	21.5	9	6.2	750	0.45		
materials prepared with F127 as a template, KCl, and with swelling agents															
LP-FDU-12[26]	1	0.0040	0.51 (TMB)	3.51	0	6.13	170	15/170	32.9	18	5.3	426	0.87		
FDU-12[27]	1	0.0040	2.13 (Xylene)	1.75	0	6.03	168	14/100	40.3	19.4	9.1	378	0.41	0.12	
materials prepared with other templates															
SBA-12[43]	1	0.0585 (Brij76[g])	0	0	0	2.35	53	RT/100	8.2	2.4	3.4	610	0.29		
FDU-1[41]	1	0.0074 (B50−6600[h])	0	0	0	6	155	25/100	23.6	12	4.7	820	0.68	0.25	[k]

[a]Temperature of synthesis/(hydro)thermal treatment at elevated temperature. [b]Unit cell parameter. [c]Pore diameter based on the NLDFT analysis for adsorption or as represented in the references. [d]Wall thickness is determined based on pore diameter and unit cell parameter of a $Fm\bar{3}m$ structured material: $W_t = (a/\sqrt{2}) - d_p$. [e]Total pore volume. [f]Volume of micropores and small mesopore, calculated using the t-plot method (see the Supporting Information Figure S9). [g]Brij76 ($C_{18}EO_{10}$). [h]B50−6600 ($EO_{39}BO_{47}EO_{39}$). [i]Negligible volume of small mesopores. [j]Small mesopores mainly. [k]Micropore volume including the volume of the interconnecting pores, if the latter are of a diameter below 4 nm.[41]

DOI: 10.1021/acs.chemmater.5b01772
Chem. Mater. 2015, 27, 5161−5169

Increasing the aging temperature to 50 °C resulted in a larger hysteresis loop (Figure 5B). The COK-19-50C material has a mesopore size of 9.4 nm and a mesopore volume of 0.32 cm^3 g^{-1}. Such a temperature induced increase of mesopore diameter and volume is commonly observed in Pluronic based synthesis and has been ascribed to an increased hydrophobicity of the EO moieties, expanding the size of the micellar core.[37−41] COK-19-50C contains a volume of 0.46 cm^3 g^{-1} of smaller mesopores (~2.5 nm) and almost no micropores, resulting in a total pore volume of 0.78 cm^3 g^{-1} (Table 1). The significant increase of pore volume compared to the sample aged at room temperature and the presence of small mesopores can be interpreted as follows. Owing to the swelling of the individual micelles, upon stacking some spaces are left between the core−shell Pluronic-silica particles, giving rise to small mesopores. The pore size distribution is shown in the inset of Figure 5B.

Incrementing the aging temperature further to 70 °C increased the mesopore size to 11.2 nm and the mesopore volume to 0.63 cm^3 g^{-1}. The size of the small mesopores was also increased to 3.2 nm.

From the pore size distribution (Table 1) and the unit cell parameter *a* derived from SAXS, the wall thickness was estimated to be approximately 8−9 nm for all materials, aged at different temperatures. These large wall thicknesses, together with a high degree of silica condensation, according to ^{29}Si NMR, are expected to contribute high mechanical stability to these materials.[42]

In order to investigate the pore structure of the material in more detail, electron tomography was performed on the sample aged at room temperature as well as at 70 °C (COK-19-70C). From the tomographic reconstructions, an arrangement of the pores consistent with the proposed structure model can be resolved in 3D (Figure 6, Figures S3−S7 and a rotating 3D representation in the Supporting Information). The mesopores in the sample aged at room temperature are smaller and more separated by pore walls compared to the pores in the sample aged at 70 °C. Tomography shows the COK-19 material has isolated spherical mesopores, separated by a thick silica wall, whereas the material aged at 70 °C shows some of these mesopores are interconnected. Moreover, these mesopores are stacked in a cubic order. When temperature is increased during the aging process, pore sizes increase and stacking is less ordered, causing some of these pores to connect. Electron tomography thus corroborates characterization with SAXS and nitrogen sorption.

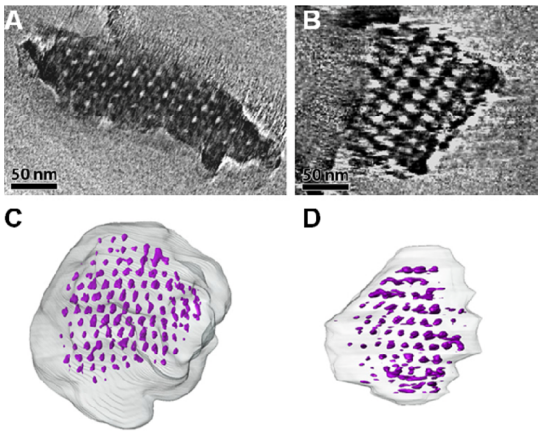

Figure 6. Pore structure of COK-19 (A, C) and COK-19-70C (B, D) revealed by orthoslices through the electron tomography reconstructions, A and B, and as segmentations of the pores, shown in purple, C and D. All four views are along a [111] direction, and the arrangement of pores is consistent with cubic close packing. In COK-19, the pores are well separated, whereas in the COK-19-70C sample some of the pores are interconnected. A rotating representation of the pore structure is provided in the Supporting Information.

Table 1 gives an overview of $Fm\bar{3}m$ ordered mesoporous materials reported in literature, synthesized using F127 (KIT-5 and FDU-12) or other amphiphilic surfactant templates such as Brij76 (SBA-12) and B-50−6600 (FDU-1). COK-19 is crystallized in circum neutral conditions, while the materials from literature are typically synthesized in hydrochloric acid environment. The materials from literature have been reported to be intergrown structures, combining cubic with hexagonal symmetry,[41,43] similar to the COK-19-50C and −70C. Aging at increased temperature not only increases the fraction of stacking disorders, it also dramatically increases the overall porosity. The total porous volume of COK-19 is in the range of 0.29 to 0.88 cm^3 g^{-1}, of which up to 0.46 cm^3 g^{-1} can be located in the micropores and small mesopores. Among all of the reported mesoporous silica materials, FDU-12 is the only one exhibiting similar wall thicknesses, although the unit cell dimensions and pore sizes are approximately the double of COK-19 as a result of swelling agents used in the synthesis. Besides these $Fm\bar{3}m$ type materials synthesized using amphiphilic surfactants, also cationic surfactants have been used.[36,44]

Formation Mechanism. For a deeper understanding of the material and its properties, the formation process of this material was investigated by DLS and SAXS characterization of intermediates in the COK-19 synthesis. A similar experimental setup was used to elucidate the formation mechanism of COK-12.[20] A series of samples was prepared by adding incremental amounts of sodium silicate solution to buffered F127 solution. At silicate additions of less than 70% of the nominal quantity, the synthesis mixture was optically transparent, while at higher silicate contents the mixture became turbid (Figure 7). At 70% silica addition a viscous gel was obtained, and eventually at 90% and 100% silica addition a suspension of particles was obtained. In Figure 7, the onset of sedimentation is already visible in the sample containing the total silica amount.

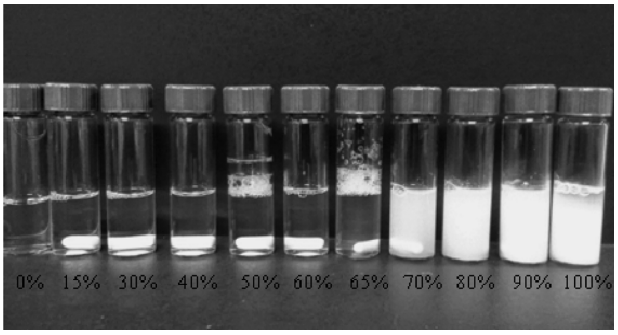

Figure 7. Photograph of the series of synthesis mixtures containing citrate buffered F127 surfactant solution and 0%, 15%, 30%, 40%, 50%, 60%, 65%, 70%, 80%, 90%, and 100% of silica addition. Photograph was taken 5 min after silicate addition.

In the citrate buffered solution, Pluronic F127 formed micelles with a hydrodynamic radius of 6.6 nm. It is commonly known that triblock copolymers such as P123 and F127 form

DOI: 10.1021/acs.chemmater.5b01772
Chem. Mater. 2015, 27, 5161−5169

spherical micelles in dilute aqueous solutions.[23] These micelles are composed of a dense core of hydrophobic PPO moieties, which are sterically stabilized by a diffuse shell of PEO chains.[23] When up to 50% of the total silica amount is added to the buffered F127 solution, the radius of the particles increases slightly with a few nanometers (Table 2, Figure S10).

Table 2. Size Estimation from SAXS and DLS of F127-Silica Core-Shell Micelles Prepared Using Different Percentages of Silica Addition

	DLS	$SAXS_{Polydisperse\ Core-Shell\ Particles}$		
% Si	R_h (nm)	R_{core} (nm)	t_{SiO_2} (nm)	R_{total} (nm)
0%	6.6			
15%	8.4	5.6	1.0	6.7
30%	9.0	5.2	3.1	8.3
40%	9.2	5.1	3.6	8.7
50%	9.4	4.6	4.1	8.7
60%	13.2	4.8	4.0	8.8
65%	36.6	4.9	4.2	9.1
70%		4.8	4.3	9.1
80%		6.2	4.6	10.8
90%		7.7	3.9	11.6
100%		4.7	4.0	8.7

Scanning transmission electron microscopy (STEM) of an evaporated synthesis mixture with 50% silicate addition confirmed the formation of spherical nanoparticles. The bright field STEM micrograph (Figure 8) shows loosely aggregated,

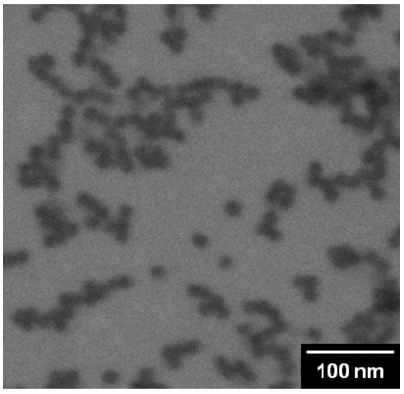

Figure 8. Bright field STEM image of F127 micelles, to which only 50% of the nominal silicate quantity was added.

monodisperse spherical nanoparticles with radii of ca. 8.5 nm. Increasing the silica concentration further led to a further increase in particle size. However, DLS was limited to samples with 65% of the total silica amount. Higher silica amounts led to a sharp transition of more aggregated particles, which could not be monitored with DLS. Using SAXS, these nanostructures could be analyzed by modeling the scattering patterns with spherical core−shell models, giving additional information on shape, inner structure, and aggregation state.

In the initial buffered F127 solution, the scattering contrast between the aqueous environment and the F127 micelles was insufficient to enable recording a SAXS pattern. SAXS patterns of synthesis mixtures with 15% up to 100% of the nominal silicate content are presented in Figure 9. At silicate contents below 65%, the scattering curves could be described by a spherical core−shell model, in which the electron density of the

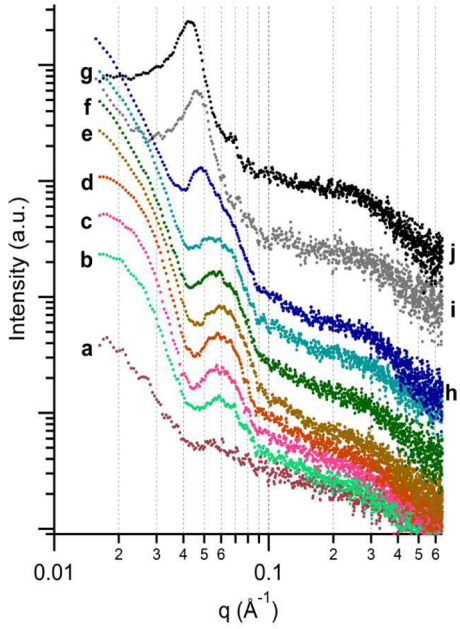

Figure 9. SAXS patterns of synthesis mixtures consisting of buffered F127 surfactant solutions to which an increasing amount of sodium silicate was added: (a) 15%, (b) 30%, (c) 40%, (d) 50%, (e) 60%, (f) 65%, (g) 70%, (h) 80%, (i) 90%, and (j) 100% of the standard synthesis. Curves were shifted vertically for clarity.

core was lower than in the shell (details provided in the Supporting Information). These differences in contrast were interpreted as a core consisting of organics surrounded by a shell containing silica. Regarding contrast, it is noteworthy that due to dilution in an aqueous solution, the presence of the organic F127 surfactant inside the pores, and an incomplete silica condensation in the final material, scattering contrast is suboptimal. After filtration and removal of the organic template through calcination, diffraction lines in the SAXS pattern are sharper and more pronounced (Figure 2).

On analogy with previously investigated P123 micelles,[20] the organic core is interpreted as the PPO part of the F127 micelle, while the shell consists of the PEO chains and infiltrated silica. An overview of estimated core radii and shell thicknesses depending on silica addition is presented in Table 2. The overall particle radii for core−shell particles, with increasing sodium silicate content, were consistent with the size estimation from DLS. DLS generally yields a slightly larger size estimate than SAXS. This discrepancy is caused by the presence of a solvation layer, reducing the diffusivity and increasing the size of particles in DLS measurements.

SAXS patterns and model fittings are shown in Figures 9 and 10 and Figures S11−S21 in the Supporting Information. The high q part of the residual (q values > 0.2 A^{-1}) additionally displayed the fingerprint of subnanometer particles. Combination of such interpretation with the core−shell micelle description led to a size estimation of nanoparticles of approximately 0.6 nm. Previously, similarly sized silica nanoparticles have been observed in SAXS studies of zeolite formation processes and have been identified as partially condensed silicate oligomer aggregates from which crystallization originates.[45−47] In the present system, it seems these silicate oligomers are the micelle infiltrating species. This interpretation was supported by the observation that the scattering intensity at q values > 0.2 A^{-1} assigned to silica

DOI: 10.1021/acs.chemmater.5b01772
Chem. Mater. 2015, 27, 5161−5169

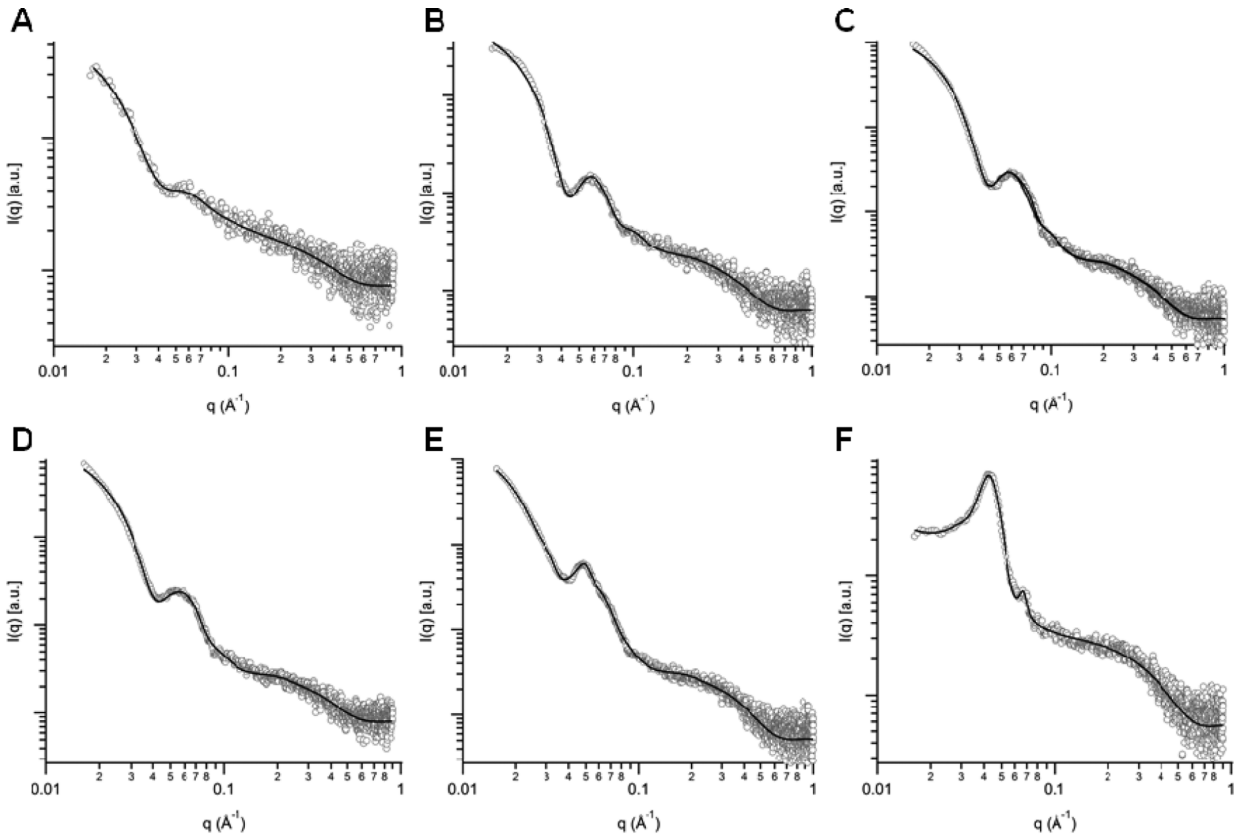

Figure 10. SAXS patterns of F127 surfactant solutions to which (A) 15%, (B) 40%, (C) 60%, (D) 70%, (E) 80%, and (F) 100% of the total sodium silicate amount in a standard synthesis was added and corresponding fitting with core–shell micelle model and unassociated silica nanoparticles. Patterns A, B, and C were fitted with a combined model for polydisperse core–shell particles and smaller, dense spherical particles. Patterns D, E, and F were fitted with the same model superimposed with pseudo-Voigt peaks (supplementary modeling information can be found in the Supporting Information).

nanoparticles did not change with increasing silica content. Silica nanoparticles formed in solution infiltrate the PEO fuzzy layer of F127 micelles and precipitate forming a capsule. Similar spherical silica infiltrated micelles were observed using P123 triblock copolymer in the formation of hexagonally ordered mesoporous silica materials.[12,20] As silica is added, more silica is concentrated in the hydrophilic PEO layer, increasing the shell thickness, slightly compressing the PPO core (Table 1).

The addition of 70% and higher percentages of the silica caused spontaneous aggregation of the silica coated F127 micelles. In SAXS, a structuring factor appeared in the small angle scattering patterns, which was modeled using pseudo-Voigt peaks. The introduction of pseudo-Voigt peaks in the model corresponds to the appearance of Bragg diffraction. Suspensions with 80% up to 100% silicate addition required three pseudo-Voigt peaks to adequately describe the SAXS patterns. The scattering intensity at q values > 0.2 A^{-1} remained constant, whereas, relatively, the amount of scattering from core–shell particles decreased. This suggests selective involvement of the core–shell micellar structures in the assembly process.

From this series of SAXS experiments and the previously illustrated COK-12 formation mechanism,[20] the following formation mechanism is proposed (Figure 11). When the highly alkaline sodium silicate solution is added to the citrate buffered F127 solution, silicate anions are protonated and form neutral silicate oligomers and orthosilicic acid $Si(OH)_4$. These small oligomers condense to larger oligomers with radii of 0.6 nm. The silicate oligomers interact strongly with the PEO tails of the Pluronic micelles, condensing in between the diffuse layer of PEO chains.[12,48,49]

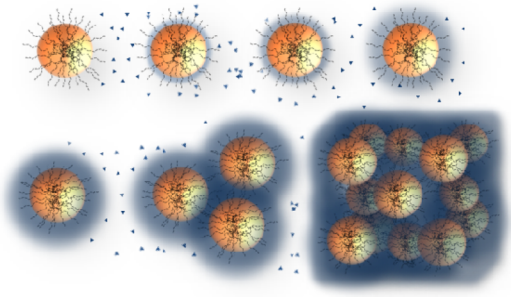

Figure 11. Schematic representation of COK-19 formation mechanism, showing the effect of increased silica concentration. Silica (blue) is precipitated on the PEO chains of the Pluronic F127 micelles (brown). The silica layer around the F127 micelles will increase in thickness until sterical stabilization is overcome and spherical silica coated micelles start to aggregate, ultimately stacking in a cubically ordered structure.

The synthesis was performed at pH 5, close to the isoelectric point of F127. The absence of charge, together with the large salt concentration, implies stabilization of the F127 micelles must occur through sterical effects of the PEO chains. With increasing sodium silicate concentration, larger amounts of silica are incorporated in the PEO layer, increasing the shell

DOI: 10.1021/acs.chemmater.5b01772
Chem. Mater. 2015, 27, 5161–5169

thickness around the micelles. It is interesting to note that in the COK-12 formation, sterical stabilization was overcome after adding only 15% of the nominal silica amount, transforming the coated, spherical micelles into elongated cylinders. In contrast, the silica coated Pluronic F127 micelles omit to form a cylindrical intermediate and form a regular arrangement of close packed silica coated spheres. As the main difference between both syntheses is the length of the PEO chains of the Pluronic surfactants (EO_{20} versus EO_{102} for, respectively, P123 and F127), the difference in sterical stabilization and consequently the different self-assembly process must be attributed to the increasing chain length.

CONCLUSIONS

By replacing the P123 Pluronic with the F127 as a template in the formation of mesoporous silica, a new ordered material was discovered. This COK-19 material has a $Fm\bar{3}m$ symmetry with hcp intergrowths, which increase with increasing temperature. The material contains spherical mesopores of 7−11 nm, interconnected via micropores and small mesopores in its 8−9-nm-thick silica walls, which could be tuned via varying aging temperature.

Intermediates in the formation process of the COK-19 material could be investigated by limiting the silicon source and modeling the SAXS pattern. Uncharged F127 micelles are wrapped with silica by accumulation of the silicate oligomers in the hydrophilic PEO layer of the micelles. Sterical stabilization decreased with increasing amounts of silica, until F127 core−silica shell particles self-assemble in a cubic close packed organization, ultimately forming the COK-19 material.

ASSOCIATED CONTENT

Supporting Information

The Supporting Information is available free of charge on the ACS Publications website at DOI: 10.1021/acs.chemmater.5b01772.

SAXS of calcined and as synthesized COK-19 materials, aged at different temperatures; TEM images of the COK-19 material; electron tomography images showing the pore structure at different angles; ^{29}Si MAS NMR of the COK-19 material; t-plot analysis of COK-19-70C; and formation mechanism DLS analysis and supplementary SAXS modeling information (PDF)

Clip showing a 3D rotating representation of the COK-19 pore structure (MPG)

Clip showing a 3D rotating representation of the COK-19-70C pore structure (MPG)

AUTHOR INFORMATION

Corresponding Author

*E-mail: Johan.Martens@biw.kuleuven.be.

Notes

The authors declare no competing financial interest.

ACKNOWLEDGMENTS

J.A.M. acknowledges the Flemish government for long-term structural funding (Methusalem, METH/08/04). The Belgian government is acknowledged for financing the interuniversity poles of attraction (IAP-PAI, P7/05 FS2). G.V.T., S.B. and T.W. acknowledge financial support from European Research Council (ERC Starting Grant no. 335078-COLOURATOMS). E.B. acknowledges financial support the Flemish FWO for a postdoctoral fellowship (1265013N). The authors gratefully thank Kristof Houthoofd for performing the NMR experiments.

REFERENCES

(1) Corma, A. From Microporous to Mesoporous Molecular Sieve Materials and Their Use in Catalysis. *Chem. Rev.* **1997**, *97*, 2373−24201.

(2) Zhao, D. Y.; Feng, J. L.; Huo, Q. S.; Melosh, N.; Fredrickson, G. H.; Chmelka, B. F.; Stucky, G. D. Triblock copolymer syntheses of mesoporous silica with periodic 50 to 300 angstrom pores. *Science* **1998**, *279*, 548−552.

(3) Zhao, D. Y.; Huo, Q. S.; Feng, J. L.; Chmelka, B. F.; Stucky, G. D. Nonionic triblock and star diblock copolymer and oligomeric surfactant syntheses of highly ordered, hydrothermally stable, mesoporous silica structures. *J. Am. Chem. Soc.* **1998**, *120*, 6024−6036.

(4) Davis, M. E. Ordered porous materials for emerging applications. *Nature* **2002**, *417*, 813−821.

(5) Vallet-Regi, M.; Ruiz-Gonzalez, L.; Izquierdo-Barba, I.; Gonzalez-Calbet, J. M. Revisiting silica based ordered mesoporous materials: medical applications. *J. Mater. Chem.* **2006**, *16*, 26−31.

(6) Mellaerts, R.; Mols, R.; Jammaer, J. A. G.; Aerts, C. A.; Annaert, P.; Van Humbeeck, J.; Van den Mooter, G.; Augustijns, P.; Martens, J. A. Increasing the oral bioavailability of the poorly water soluble drug itraconazole with ordered mesoporous silica. *Eur. J. Pharm. Biopharm.* **2008**, *69*, 223−230.

(7) Mellaerts, R.; Roeffaers, M. B. J.; Houthoofd, K.; Van Speybroeck, M.; De Cremer, G.; Jammaer, J. A. G.; Van den Mooter, G.; Augustijns, P.; Hofkens, J.; Martens, J. A. Molecular organization of hydrophobic molecules and co-adsorbed water in SBA-15 ordered mesoporous silica material. *Phys. Chem. Chem. Phys.* **2011**, *13*, 2706−2713.

(8) Van Speybroeck, M.; Barillaro, V.; Thi, T. D.; Mellaerts, R.; Martens, J.; Van Humbeeck, J.; Vermant, J.; Annaert, P.; Van Den Mooter, G.; Augustijns, P. Ordered Mesoporous Silica Material SBA-15: A Broad-Spectrum Formulation Platform for Poorly Soluble Drugs. *J. Pharm. Sci.* **2009**, *98*, 2648−2658.

(9) Mellaerts, R.; Aerts, C. A.; Humbeeck, J. V.; Augustijns, P.; den Mooter, G. V.; Martens, J. A. Enhanced release of itraconazole from ordered mesoporous SBA-15 silica materials. *Chem. Commun.* **2007**, 1375−1377.

(10) Monnier, A.; Schüth, F.; Huo, Q.; Kumar, D.; Margolese, D.; Maxwell, R. S.; Stucky, G. D.; Krishnamurty, M.; Petroff, P.; Firouzi, A.; Janicke, M.; Chmelka, B. F. Cooperative Formation of Inorganic-Organic Interfaces in the Synthesis of Silicate Mesostructures. *Science* **1993**, *261*, 1299−1303.

(11) Huo, Q.; Margolese, D. I.; Ciesla, U.; Feng, P.; Gier, T. E.; Sieger, P.; Leon, R.; Petroff, P. M.; Schuth, F.; Stucky, G. D. Generalized synthesis of periodic surfactant/inorganic composite materials. *Nature* **1994**, *368*, 317−321.

(12) Mesa, M.; Sierra, L.; Guth, J. L. Contribution to the study of the formation mechanism of mesoporous SBA-15 and SBA-16 type silica particles in aqueous acid solutions. *Microporous Mesoporous Mater.* **2008**, *112*, 338−350.

(13) Yuan, P.; Yang, J.; Bao, X. J.; Zhao, D. Y.; Zou, J.; Yu, C. Z. Highly Ordered Cubic Mesoporous Materials with the Same Symmetry but Tunable Pore Structures. *Langmuir* **2012**, *28*, 16382−16392.

(14) Ciesla, U.; Schüth, F. Ordered mesoporous materials. *Microporous Mesoporous Mater.* **1999**, *27*, 131−149.

(15) Kresge, C. T.; Leonowicz, M. E.; Roth, W. J.; Vartuli, J. C.; Beck, J. S. Ordered mesoporous molecular sieves synthesized by a liquid-crystal template mechanism. *Nature* **1992**, *359*, 710−712.

(16) Beck, J. S.; Vartuli, J. C.; Roth, W. J.; Leonowicz, M. E.; Kresge, C. T.; Schmitt, K. D.; Chu, C. T. W.; Olson, D. H.; Sheppard, E. W. A new family of mesoporous molecular sieves prepared with liquid crystal templates. *J. Am. Chem. Soc.* **1992**, *114*, 10834−10843.

(17) Meynen, V.; Cool, P.; Vansant, E. F. Verified syntheses of mesoporous materials. *Microporous Mesoporous Mater.* **2009**, *125*, 170−223.

DOI: 10.1021/acs.chemmater.5b01772
Chem. Mater. 2015, 27, 5161−5169

(18) Kleitz, F.; Liu, D.; Anilkumar, G. M.; Park, I.-S.; Solovyov, L. A.; Shmakov, A. N.; Ryoo, R. Large Cage Face-Centered-Cubic Fm3m Mesoporous Silica: Synthesis and Structure. *J. Phys. Chem. B* **2003**, *107*, 14296−14300.
(19) Jammaer, J.; Aerts, A.; D'Haen, J.; Seo, J. W.; Martens, J. A. Convenient synthesis of ordered mesoporous silica at room temperature and quasi-neutral pH. *J. Mater. Chem.* **2009**, *19*, 8290−3.
(20) Jammaer, J.; van Erp, T. S.; Aerts, A.; Kirschhock, C. E. A.; Martens, J. A. Continuous Synthesis Process of Hexagonal Nanoplates of P6m Ordered Mesoporous Silica. *J. Am. Chem. Soc.* **2011**, *133*, 13737−13745.
(21) Liu, J.; Yang, Q.; Zhao, X. S.; Zhang, L. Pore size control of mesoporous silicas from mixtures of sodium silicate and TEOS. *Microporous Mesoporous Mater.* **2007**, *106*, 62−67.
(22) Alexandridis, P.; Alan Hatton, T. Poly(ethylene oxide)-poly(propylene oxide)-poly(ethylene oxide) block copolymer surfactants in aqueous solutions and at interfaces: thermodynamics, structure, dynamics, and modeling. *Colloids Surf., A* **1995**, *96*, 1−46.
(23) Alexandridis, P.; Holzwarth, J. F.; Hatton, T. A. Micellization of Poly(ethylene oxide)-Poly(propylene oxide)-Poly(ethylene oxide) Triblock Copolymers in Aqueous Solutions: Thermodynamics of Copolymer Association. *Macromolecules* **1994**, *27*, 2414−2425.
(24) Mortensen, K. Structural studies of aqueous solutions of PEO - PPO - PEO triblock copolymers, their micellar aggregates and mesophases; a small-angle neutron scattering study. *J. Phys.: Condens. Matter* **1996**, *8*, A103.
(25) Zhao, D.; Huo, Q.; Feng, J.; Chmelka, B. F.; Stucky, G. D. Nonionic Triblock and Star Diblock Copolymer and Oligomeric Surfactant Syntheses of Highly Ordered, Hydrothermally Stable, Mesoporous Silica Structures. *J. Am. Chem. Soc.* **1998**, *120*, 6024−6036.
(26) Cao, L.; Kruk, M. Short synthesis of ordered silicas with very large mesopores. *RSC Adv.* **2014**, *4*, 331−339.
(27) Huang, L.; Yan, X.; Kruk, M. Synthesis of Ultralarge-Pore FDU-12 Silica with Face-Centered Cubic Structure. *Langmuir* **2010**, *26*, 14871−14878.
(28) Fan, J.; Yu, C.; Gao, F.; Lei, J.; Tian, B.; Wang, L.; Luo, Q.; Tu, B.; Zhou, W.; Zhao, D. Cubic Mesoporous Silica with Large Controllable Entrance Sizes and Advanced Adsorption Properties. *Angew. Chem., Int. Ed.* **2003**, *42*, 3146−3150.
(29) Kleitz, F.; Kim, T.-W.; Ryoo, R. Phase Domain of the Cubic Im$\bar{3}$m Mesoporous Silica in the EO106PO70EO106−Butanol−H2O System. *Langmuir* **2006**, *22*, 440−445.
(30) Wan, Y.; Shi, Y.; Zhao, D. Designed synthesis of mesoporous solids via nonionic-surfactant-templating approach. *Chem. Commun.* **2007**, 897−926.
(31) Kline, S. R. Reduction and analysis of SANS and USANS data using IGOR Pro. *J. Appl. Crystallogr.* **2006**, *39*, 895−900.
(32) Bartlett, P.; Ottewill, R. H. A neutron scattering study of the structure of a bimodal colloidal crystal. *J. Chem. Phys.* **1992**, *96*, 3306−3318.
(33) Förster, S.; Timmann, A.; Konrad, M.; Schellbach, C.; Meyer, A.; Funari, S. S.; Mulvaney, P.; Knott, R. Scattering Curves of Ordered Mesoscopic Materials. *J. Phys. Chem. B* **2005**, *109*, 1347−1360.
(34) Ruland, W.; Smarsly, B. M. Two-dimensional small-angle X-ray scattering of self-assembled nanocomposite films with oriented arrays of spheres: determination of lattice type, preferred orientation, deformation and imperfection. *J. Appl. Crystallogr.* **2007**, *40*, 409−417.
(35) Warren, B. E. *X-ray Diffraction*; Addison-Wesley Pub. Co.: Reading, MA, 1969.
(36) Miyasaka, K.; Han, L.; Che, S.; Terasaki, O. A Lesson from the Unusual Morphology of Silica Mesoporous Crystals: Growth and Close Packing of Spherical Micelles with Multiple Twinning. *Angew. Chem., Int. Ed.* **2006**, *45*, 6516−6519.
(37) Galarneau, A.; Cambon, H.; Di Renzo, F.; Ryoo, R.; Choi, M.; Fajula, F. Microporosity and connections between pores in SBA-15 mesostructured silicas as a function of the temperature of synthesis. *New J. Chem.* **2003**, *27*, 73−79.
(38) Ryoo, R.; Ko, C. H.; Kruk, M.; Antochshuk, V.; Jaroniec, M. Block-Copolymer-Templated Ordered Mesoporous Silica: Array of Uniform Mesopores or Mesopore−Micropore Network? *J. Phys. Chem. B* **2000**, *104*, 11465−11471.
(39) Stevens, W. J. J.; Lebeau, K.; Mertens, M.; Van Tendeloo, G.; Cool, P.; Vansant, E. F. Investigation of the Morphology of the Mesoporous SBA-16 and SBA-15 Materials. *J. Phys. Chem. B* **2006**, *110*, 9183−9187.
(40) Hoang, V.-T.; Huang, Q.; Eić, M.; Do, T.-O.; Kaliaguine, S. Structure and Diffusion Characterization of SBA-15 Materials. *Langmuir* **2005**, *21*, 2051−2057.
(41) Matos, J. R.; Kruk, M.; Mercuri, L. P.; Jaroniec, M.; Zhao, L.; Kamiyama, T.; Terasaki, O.; Pinnavaia, T. J.; Liu, Y. Ordered Mesoporous Silica with Large Cage-Like Pores: Structural Identification and Pore Connectivity Design by Controlling the Synthesis Temperature and Time. *J. Am. Chem. Soc.* **2002**, *125*, 821−829.
(42) Zhao, D.; Wan, Y.; Zhou, W. *Ordered Mesoporous Materials*; Wiley-VCH Verlag GmbH & Co. KGaA: Weinheim, Germany, 2013; pp 5−54.
(43) Sakamoto, Y.; Díaz, I.; Terasaki, O.; Zhao, D.; Pérez-Pariente, J.; Kim, J. M.; Stucky, G. D. Three-Dimensional Cubic Mesoporous Structures of SBA-12 and Related Materials by Electron Crystallography. *J. Phys. Chem. B* **2002**, *106*, 3118−3123.
(44) Shi, C.; Deng, S.; Wang, J.; Sun, P.; Chen, T. Hierarchically mesoporous silica single-crystalline nanorods with three dimensional cubic Fm-3m mesostructure. *J. Mater. Chem. A* **2013**, *1*, 14555−14561.
(45) Aerts, A.; Follens, L. R. A.; Haouas, M.; Caremans, T. P.; Delsuc, M.-A.; Loppinet, B.; Vermant, J.; Goderis, B.; Taulelle, F.; Martens, J. A.; Kirschhock, C. E. A. Combined NMR, SAXS, and DLS Study of Concentrated Clear Solutions Used in Silicalite-1 Zeolite Synthesis. *Chem. Mater.* **2007**, *19*, 3448−3454.
(46) Aerts, A.; Haouas, M.; Caremans, T. P.; Follens, L. R. A.; van Erp, T. S.; Taulelle, F.; Vermant, J.; Martens, J. A.; Kirschhock, C. E. A. Investigation of the Mechanism of Colloidal Silicalite-1 Crystallization by Using DLS, SAXS, and 29Si NMR Spectroscopy. *Chem. - Eur. J.* **2010**, *16*, 2764−2774.
(47) Castro, M.; Haouas, M.; Taulelle, F.; Lim, I.; Breynaert, E.; Brabants, G.; Kirschhock, C. E. A.; Schmidt, W. Multidiagnostic analysis of silicate speciation in clear solutions/sols for zeolite synthesis. *Microporous Mesoporous Mater.* **2014**, *189*, 158−162.
(48) Flodström, K.; Teixeira, C. V.; Amenitsch, H.; Alfredsson, V.; Lindén, M. In Situ Synchrotron Small-Angle X-ray Scattering/X-ray Diffraction Study of the Formation of SBA-15 Mesoporous Silica. *Langmuir* **2004**, *20*, 4885−4891.
(49) Liu, J.; Yang, Q.; Zhang, L.; Yang, H.; Gao, J.; Li, C. Organic−Inorganic Hybrid Hollow Nanospheres with Microwindows on the Shell. *Chem. Mater.* **2008**, *20*, 4268−4275.

DOI: 10.1021/acs.chemmater.5b01772
Chem. Mater. 2015, 27, 5161−5169